Korean J. Chem. Eng., 33(6), 1846-1854 (2016)
DOI: 10.1007/s11814-016-0038-1

pISSN: 0256-1115
eISSN: 1975-7220

Catalytic activity of copper-ceria catalysts supported on different zeolites for CO oxidation

Dong Zhang, Huiping Zhang, and Ying Yan†

School of Chemistry and Chemical Engineering, South China University of Technology, Guangzhou 510640, P. R. China
(*Received 30 November 2015 • accepted 1 February 2016*)

Abstract−Copper-ceria catalysts for CO oxidation supported on 4A, 5A, NaX and NaY zeolites were prepared by incipient wetness impregnation and excess-solution impregnation. Catalysts were characterized by SEM, EDX, XRD, N_2 adsorption-desorption, H_2-TPR and XPS. Results revealed that the catalysts were greatly affected by zeolites and preparation method. EDX results indicated the metal loading of 4A-ES (5.1 wt% Cu, 15.7 wt% Ce), 5A-ES (5.9 wt% Cu, 19.2% Ce), NaX-ES (11.7 wt% Cu, 4.2 wt% Ce) and NaY-ES (11.0 wt% Cu, 7.9 wt% Ce) greatly varied. TPR results suggested that the peak at around 195 °C was presented in NaX-ES and 4A-IW, standing for dispersed copper species that is very active for CO oxidation. The catalytic activity of 4A-ES and NaX-ES was the best among catalysts made by excess-solution impregnation, demonstrated by the lowest T_{50} at 127 and 129 °C, respectively. The catalytic activity of catalysts made by incipient wetness impregnation was worse than that of catalysts made by excess-solution impregnation, examined by the T_{50} of 4A-IW and NaX-IW at 128 and 192 °C, respectively.

Keywords: CO Oxidation, Copper-ceria Catalyst, Zeolite, Incipient Wetness Impregnation, Excess-solution Impregnation

INTRODUCTION

The catalytic oxidation of CO has received much attention owing to its environmental application, including the removal of trace quantities of CO from enclosed atmospheres such as indoor parking, submarine and space crafts. CO oxidation has been carried out over noble metal catalysts [1-3] and transition metal catalysts [4,5]. Among the transition metal catalysts, copper-ceria catalysts have demonstrated promising characteristics toward CO oxidation [6-9]. Furthermore, the catalytic activity of catalysts significantly depends on the contacting efficiency, in which the support and the preparation method play crucial roles.

Various supports have been developed for catalysts including alumina [10], silica [11], glass fibers [12] and zeolites [2,13,14]. Zeolites offer large surface area, uniform pore structure and special characteristic, and thereby are considered as preferred supports. Hiroshi [15] made Pt-loaded catalysts on 4A, NaX and mordenite zeolite for CO selective oxidation from hydrogen-rich fuels and found that the Pt-loaded mordenite show highest selectivity and conversion. Kolobova [16] prepared Ag/ZSM-5 zeolite catalysts for CO oxidation and found these catalysts had good reproducibility and stability. Lin [2] synthesized Au/NaY zeolite-supported catalyst for CO oxidation. Among zeolites, LTA (4A, 5A) and FAU (NaX, NaY) zeolites have been widely used as supports for catalysts [17-20] owing to the high thermal stability, large surface area and shape selectivity. However, the copper-ceria catalysts for CO oxidation supported on LTA and FAU zeolites have not been prepared. The effects of zeolite support on the characteristics of catalysts had not been systematically investigated either. Moreover, the structural, morphological and catalytic properties of copper-ceria catalysts are greatly affected by preparation method. Conventionally, incipient wetness impregnation is frequently used to prepare the supported catalysts. Bowker [21], Junges [22] and Soares [23] prepared supported catalysts for CO oxidation using incipient wetness impregnation. However, the active metal species could not be uniformly distributed due to capillary action in incipient wetness impregnation. In contrast, for excess-solution impregnation, diffusion is the main force dispersing active metal precursors, leading to well-dispersed metal species.

The aim of this work was to compare the catalytic activity of CO on the copper-ceria catalysts supported on different zeolites. Then, the effects of excess-solution impregnation and incipient wetness impregnation on the properties of catalysts were also explored.

EXPERIMENTAL

1. Materials

$Cu(NO_3)_2{\cdot}3H_2O$ (≥99.0%, Guangzhou Chemical Reagent Factory); $Ce(NO_3)_3{\cdot}6H_2O$ (≥99.0%, Tianjin Kermel Reagent Co., Ltd.); 4A zeolite (250-425 μm, Tianjin Kermel Reagent Co., Ltd.); 5A zeolite (250-425 μm, Tianjin Kermel Reagent Co., Ltd.); NaX zeolite (250-425 μm, Anhui Mingmei Co., Ltd.); NaY zeolite (250-425 μm, Pingxiang Xintao Co., Ltd.); CO/Air mixture (180 ppm, Guangzhou Zhuozheng Air Co., Ltd.).

2. Preparation of Catalysts

The catalysts were prepared using excess-solution impregnation and incipient wetness impregnation. Zeolites were pretreated at 300 °C for 2 h in air to remove any adsorbed moisture. In the case

†To whom correspondence should be addressed.
E-mail: yingyan@scut.edu.cn

of excess-solution impregnation, 22.0 g $Ce(NO_3)_3{\cdot}6H_2O$ and 7.0 g $Cu(NO_3)_2{\cdot}3H_2O$ were dissolved into 90.0 mL deionized water. 5 g zeolites were added into the solution under vigorous stirring (10 min) and further impregnated for 12 h at room temperature. Then, the catalyst precursors were filtered and dried at 150 °C for 2 h. For incipient wetness impregnation, the calculated amount of $Ce(NO_3)_3{\cdot}6H_2O$ and $Cu(NO_3)_2{\cdot}3H_2O$ according to the EDX results was dissolved in a certain amount of deionized water, which was fully soaked by 5 g zeolites. For example, to prepare 4A zeolite-supported catalyst by incipient wetness impregnation, 1.30 g $Cu(NO_3)_2{\cdot}3H_2O$ and 3.27 g $Ce(NO_3)_3{\cdot}6H_2O$ were dissolved in 7.00 g deionized water in order to be absorbed by 5 g 4A zeolite. To prepare NaX zeolite-supported catalyst, 2.77 g $Cu(NO_3)_2{\cdot}3H_2O$ and 0.81 g $Ce(NO_3)_3{\cdot}6H_2O$ were dissolved in 7.30 g deionized water to be absorbed by 5 g NaX zeolite. For example, to prepare 4A zeolite-supported catalyst by incipient wetness impregnation, 1.30 g $Cu(NO_3)_2{\cdot}3H_2O$ and 3.27 g $Ce(NO_3)_3{\cdot}6H_2O$ were dissolved in 7.00 g deionized water in order to be absorbed by 5 g 4A zeolite. To prepare NaX zeolite-supported catalyst, 2.77 g $Cu(NO_3)_2{\cdot}3H_2O$ and 0.81 g $Ce(NO_3)_3{\cdot}6H_2O$ were dissolved in 7.30 g deionized water to be absorbed by 5 g NaX zeolite. Then, the catalyst precursors were placed at room temperature for 12 h. Finally, all as-prepared precursors were dried at 150 °C for 2 h and calcined at 400 °C in air for 2 h. Catalysts supported on the specific zeolite prepared by excess-solution impregnation or incipient wetness impregnation were denoted as *zeolite type*-ES or -IW, respectively. For instance, 4A-ES stands for the catalysts supported on 4A zeolite by excess-solution impregnation.

3. Characterization

X-ray diffraction patterns of samples were obtained on a D8 Advance (Bruker Co.) diffractometer using Cu Kα radiation (40 kV, 40 mA). The specific surface area and pore size distribution of samples were measured using ASAP 2020 analyzer (Micromeritics) at 77 K. The morphology and chemical composition of samples were determined using a MERLIN scanning electron microscope Gemini (Zeiss Co.) equipped with an energy dispersive X-ray spectrometer (EDX) coupled with the microscope chamber. H_2-Temperature programmed reduction tests were conducted on Quantachrome automated chemisorption analyzer by heating the sample in H_2 (10 vol%)/Air flow (30 mL·min^{-1}) at a heating rate of 10 °C·min^{-1} from room temperature to 700 °C. The binding energy of each element including Cu, Ce and O was analyzed using Al Kα (1486.6 eV) at 4.5 W. by X-ray photoelectron spectroscopy (XPS; PHI-X-tool, ULVAC-Phi Inc.).

4. Catalytic Activity Tests

The catalytic tests were performed in a fixed bed reactor with a stainless steel tube (10 mm i.d., 450 mm length) at atmospheric pressure. The tests were carried out under temperature-programmed condition. The temperature was automatically monitored with E-type thermocouples along the fixed bed. In each test, samples were filled into the reactor with the bed height of 10 mm. The gas mixture consisting of 180 ppm CO/Air was passed through the fixed bed at the flow rate of 100 mL·min^{-1}. A typical gas hourly space velocity (GHSV) was 7,643 h^{-1}. The outlet concentration of CO was determined by infrared gas analyzer (QGS-08B, Baif-Maihak Co.). The CO conversion was calculated based on the outlet concentration of CO.

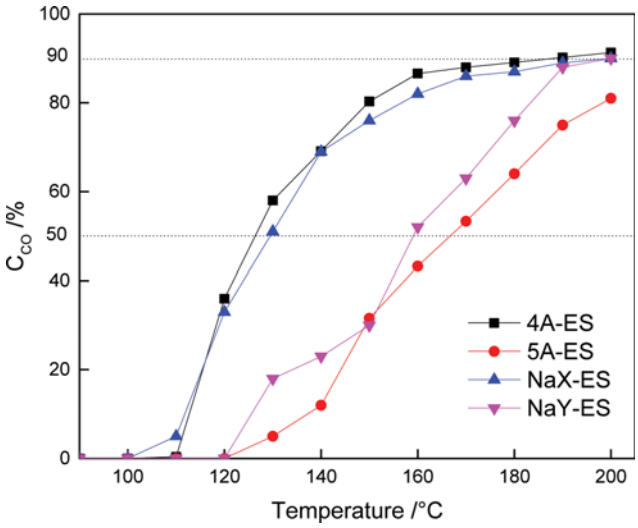

Fig. 1. Catalytic activity of catalysts made by excess-solution impregnation.

$$C_{CO}=\frac{CO_{in}-CO_{out}}{CO_{in}}\times 100\%$$

where C_{CO} represents the CO conversion, CO_{in} and CO_{out} is the inlet and outlet CO concentrations.

RESULTS AND DISCUSSION

1. Different Zeolite Supports

The catalytic performance of 4A-ES, 5A-ES, NaX-ES and NaY-ES was carried out to compare the zeolite supports on which the catalysts made by excess-solution impregnation showed best catalytic activity for the further investigation of the differences between excess-solution impregnation and incipient wetness impregnation. The result is shown in Fig. 1. The catalytic activity of zeolite supported copper-ceria catalysts increases in the order of 5A-ES< NaY-ES<NaX-ES≈4A-ES. 4A-ES and NaX-ES show the best catalytic performance. The 50% CO conversion was only 127 °C for 4A-ES and 129 °C for NaX-ES, while it was 160 and 166 °C for NaY-ES and 5A-ES. The 90% CO conversion could be reached at 200 °C for all catalysts except 5A-ES. Therefore, 4A and NaX zeolites were chosen to be the supports for 4A-IW and NaX-IW, which were to be made by incipient wetness impregnation. The metal loading of 4A-IW and NaX-IW was adjusted to be the same as 4A-ES and NaX-ES to investigate the differences between excess-solution impregnation and incipient wetness impregnation on the properties of catalysts.

2. Composition and Morphology

EDX and SEM were used to determine the chemical composition and morphology of the catalysts. Fig. 2 shows the elemental distribution of the catalysts. It can be seen that the peaks of Si, Al, O, Na, Cu and Ce were identified in all catalysts. The specific loading of Cu, Ce of the catalysts is shown in Table 1. The quantitative analysis indicated that the metal loadings on these catalysts greatly varied when using excess-solution impregnation. For 4A-ES and

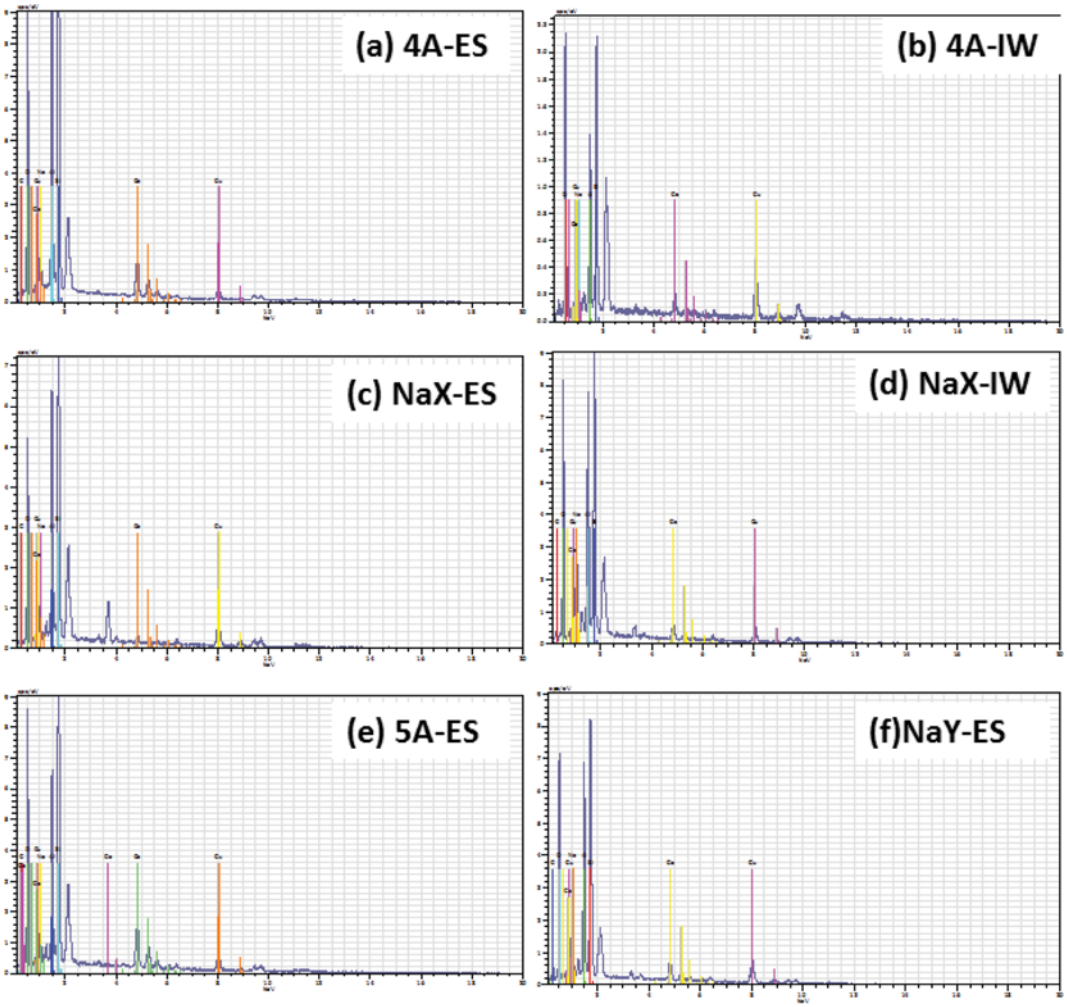

Fig. 2. EDX images of catalysts: (a) 4A-ES, (b) 4A-IW, (c) NaX-ES, (d) NaX-IW, (e) 5A-ES and (f) NaY-ES.

Table 1. Metal content of catalysts

Catalyst	Metal content (wt%)	
	Cu	Ce
4A-ES	5.1	15.7
4A-IW	6.3	17.1
5A-ES	5.9	19.2
NaX-ES	11.7	4.2
NaX-IW	10.8	5.6
NaY-ES	11.0	7.9

5A-ES, the loading of Cu (5.1, 5.9 wt%) was much lower than that of Ce (15.7, 19.2 wt%). In contrast, the loading of Cu (11.7, 11.0 wt%) was much higher than that of Ce (4.2, 7.9 wt%) for NaX-ES and NaY-ES. In excess-solution impregnation, the zeolite support and active metal cations contacted long enough to reach adsorption equilibrium, indicating the metal loadings were in the maximum amount. In excess-solution impregnation, the experimental variables—solution volume, metal concentration, impregnation duration, zeolite weight, zeolite size—were kept the same expect the zeolite type. As a result, a plausible explanation could be that zeolite type could be responsible for the different metal loading. A few studies have pointed out that the different zeolites have varied adsorption capacity towards metal ions [24-26]. Moreover, according to Hegazy [26], pure zeolite A showed a non-selective behavior while zeolite X was highly selective for Cu^{2+}, which justified the result of metal content that 4A-ES had less copper species and NaY-ES, which had the similar framework to zeolite X, had more copper species.

As can be seen in Table 1, the metal loading of the catalysts using incipient wetness impregnation was similar to that of catalysts made by excess-solution impregnation. 4A-ES had 5.1 wt% Cu and 15.7 wt% Ce, while 4A-IW had 6.3 wt% Cu and 17.1 wt% Ce. For NaX-ES and NaX-IW, the Cu and Ce loadings were 11.7 wt%, 10.8 wt% and 4.2 wt% and 5.6 wt%, respectively. Therefore, the comparison between the excess-solution and incipient wetness impregnation was believed to be reasonable since the metal loadings of sample were kept almost the same.

The SEM images of all catalysts are displayed in Fig. 3, which illustrates that all catalysts had the crystalline structure of the corresponding zeolite supports. In Fig. 3(a), (b) and (e), the cubic

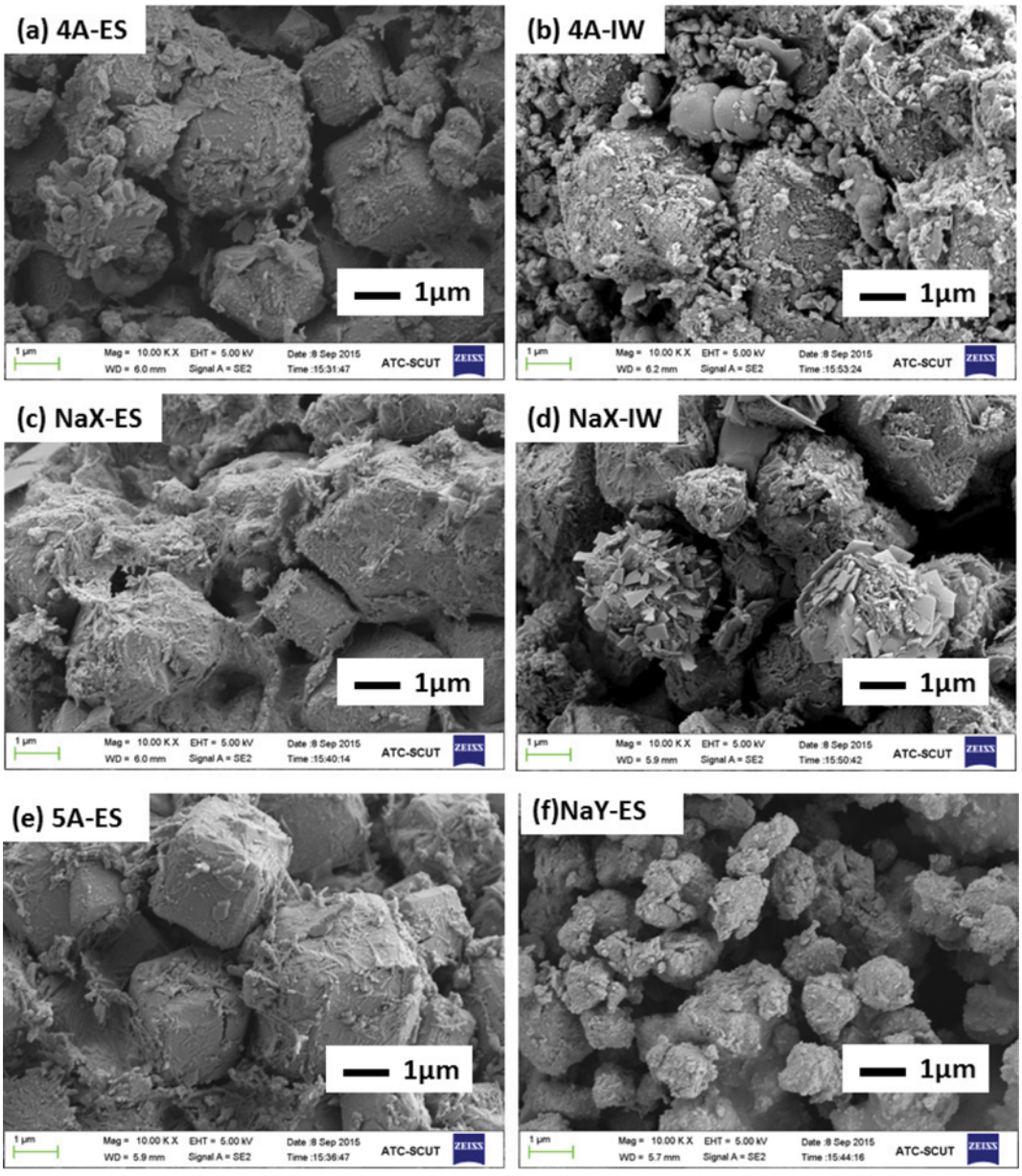

Fig. 3. SEM images of catalysts: (a) 4A-ES, (b) 4A-IW, (c) NaX-ES, (d) NaX-IW, (e) 5A-ES and (f) NaY-ES.

crystals of LTA are observed. In contrast, the faujasite structures in Fig. 3(c), (d) and (f) are not clear enough, especially for the NaY-ES because the crystal size is smaller than those of NaX-ES and NaX-IW. For all catalysts, the amorphous metal oxides are attached on the surface of zeolite crystal. In the case of catalysts made by excess-solution impregnation, the metal oxide distribution is relatively uniform, though some small clusters can be seen in all samples. Meanwhile, in Fig. 3(b), more metal clusters are attached on the surface of LTA crystal in 4A-IW in comparison with 4A-ES. Most metal clusters are in the range of 0.1-0.3 μm and are randomly dispersed on the surface of zeolite crystal, which might be preferred active sites because they can contact with CO molecules without intraparticle mass transfer resistance. Besides, in Fig. 3(d), some fragments of metal oxides appear on the surface of NaX-IW, while they can barely be seen on the NaX-ES. It can be concluded that the metal oxides are likely to be unevenly distributed by using incipient wetness impregnation.

3. XRD Patterns

XRD was used to analyze the crystallite phase of samples. XRD patterns of zeolites and catalysts are shown in Fig. 4. All XRD patterns of catalysts made by excess-solution presented the diffraction peaks matched with the patterns of corresponding zeolites, indicating the primary crystal structures of zeolites were preserved in catalysts. Meanwhile, we note that many primary peaks of zeolites in the corresponding catalysts were weakened. Some of them became unobservable. This might be because zeolite structures lose some crystallinity after ion exchange, which is likely to happen during the excess-solution impregnation. The diffraction peaks of tenorite copper oxide phase at 35.6°, 38.8° and 63.1° and those of cubic fluorite type phase of ceria at 28.5°, 33.0°, 48.7° and 56.6°

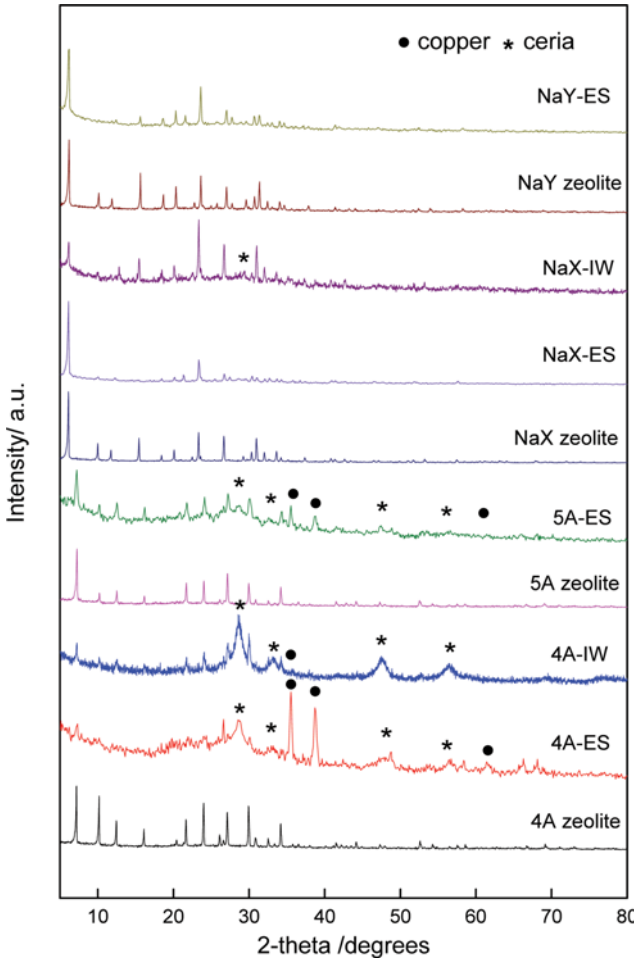

Fig. 4. XRD patterns of samples.

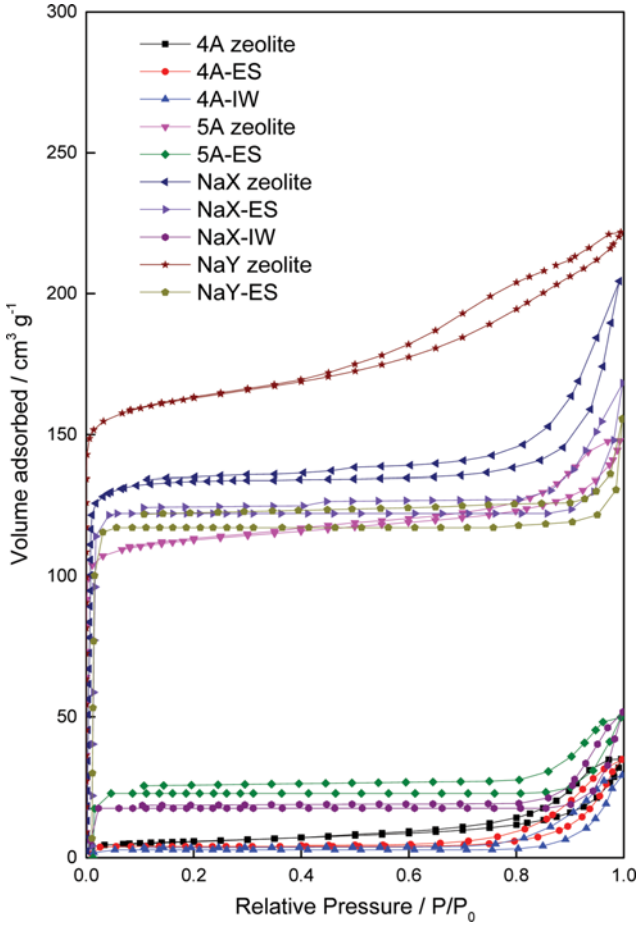

Fig. 5. N_2 adsorption-desorption isotherms of samples.

were identified [27]. It can be seen that the peaks of copper oxide and ceria were more discernible in 4A-ES and 5A-ES than NaX-ES and NaY-ES, suggesting the distribution of CuO and CeO_2 on 4A-ES and 5A-ES was less uniform than NaX-ES and NaY-ES.

A comparison of diffraction peaks between catalysts made by excess-solution impregnation and incipient wetness impregnation was also made. Compared with 4A-ES and NaX-ES, the primary diffraction peaks of zeolites in 4A-IW and NaX-IW were more discernible, suggesting more crystallinity was preserved after incipient wetness impregnation because ion exchange could hardly take place as a result of the limited solution and contact time. In addition, the random distribution of metal species, shown in SEM images of 4A-IW and NaX-IW in Fig. 3(b) and (d), contributed to the exposure of zeolite surface, which led to the more intense primary peaks. In contrast with 4A-ES, the diffraction peaks of ceria (28.5°, 33.0°, 48.7°, 56.6°) in 4A-IW were more intense, suggesting the presence of bulk CeO_2. Meanwhile, the peaks of CuO (35.6°, 38.8°, 63.1°) in 4A-IW, however, were hardly observable. This might be because CuO particle size is too small to be detected by XRD. It can be inferred that the metal clusters of 4A-IW shown in Fig. 3(b) could be the bulk CeO_2 covered with CuO species. In comparison, some peaks of CuO (35.6°, 38.8°) and CeO_2 (28.5°) became detectable in NaX-IW, indicating the presence the relatively large particles of CuO and CeO_2 compared with NaX-ES. It was corresponding with the fragment presented in Fig. 3(d). It can be concluded that, in comparison with excess-solution impregnation, the metal species were relatively unevenly dispersed when incipient wetness impregnation was used.

4. N_2 Adsorption-desorption Isotherms

N_2 adsorption-desorption isotherms were used to characterize textural properties of samples. The N_2 adsorption-desorption isotherms and pore size distribution and BET surface area for zeolites and catalysts are given in Fig. 5 and Table 2, respectively. All zeolites, except 4A zeolites, possess large BET surface area (>300 m^2). The reason why 4A zeolite had less BET surface area is that the pore openings of 4A zeolite barely adsorb any nitrogen molecules [28,29]. It also explains its low micropore volumes. In comparison with zeolites, the corresponding catalysts showed lower BET surface area, micropore and mesopore volume. This is because the pores were filled with copper and cerium species during impregnation, which might block pores and therefore reduce BET surface and pore volume. As for the catalysts made by excess-solution impregnation, the micropore volume of 4A-ES and 5A-ES was reduced dramatically compared to 4A and 5A zeolites, while there was only a slight reduction of micropore volume for NaX-ES and NaY-ES compared to NaX and NaY zeolites. A plausible explanation is that the larger pore size of NaX and NaY zeolites (0.74 nm)

Table 2. Pore structure properties of samples

Sample	Pore structure properties			
	Micropore ($cm^3 \cdot g^{-1}$)	Mesopore ($cm^3 \cdot g^{-1}$)	Total volume ($cm^3 \cdot g^{-1}$)	BET surface area ($m^2 \cdot g^{-1}$)
4A zeolite	0.08	0.053	0.055	20
4A-ES	0.006	0.049	0.054	12
4A-IW	0.0004	0.04	0.041	8
5A zeolite	0.15	0.071	0.22	392
5A-ES	0.035	0.046	0.081	67
NaX zeolite	0.21	0.11	0.32	410
NaX-ES	0.19	0.076	0.27	365
NaX-IW	0.023	0.046	0.069	51
NaY zeolite	0.21	0.13	0.34	567
NaY-ES	0.18	0.02	0.20	343

is capable of holding more copper and cerium oxides than 4A and 5A zeolites, which possess smaller pore size (0.4 and 0.5 nm). It may also explain the fact that the BET surface area of 5A-ES is much lower than 5A zeolite. Note that compared with the 4A-ES and NaX-ES, 4A-IW and NaX-IW had less BET surface area. BET surface area of 4A-IW was 8 $m^2 \cdot g^{-1}$ while that of 4A-ES was 12 $m^2 \cdot g^{-1}$. NaX-IW showed a more drastic decrease of BET surface area - 51 $m^2 \cdot g^{-1}$ compared with that of NaX-ES - 365 $m^2 \cdot g^{-1}$. The incipient wetness impregnation also led to the decrease in pore volume, especially the micropore volume, in comparison with excess-solution impregnation. This was due to the capillary action, which draws the solution into pores in incipient wetness impregnation. The pores were easily blocked by the excess metal species brought by capillary action [30]. For excess-solution process, diffusion, though slower, is the main force to load the metal species onto the surface of support. The metal species are more likely to be dispersed well rather than randomly gathered [31]. It can be concluded that excess-solution impregnation contributed to a more uniform metal species distribution and larger BET surface and pore volume in contrast to incipient wetness impregnation.

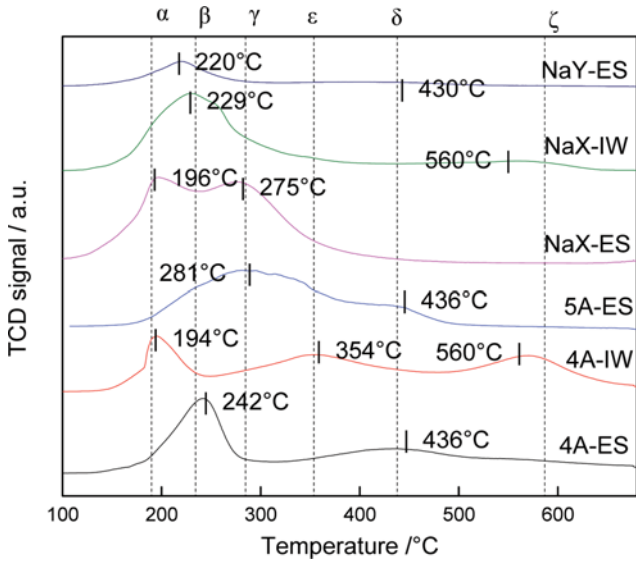

Fig. 6. H_2-TPR profiles of catalysts.

5. Temperature-programmed Reduction Performances

The reducibility of catalysts was examined by H_2-TPR. The H_2-TPR profiles are shown in Fig. 6. According to the literature [32], pure CeO_2 exhibits two reduction peaks at about 523 and 658 °C, whereas the pure CuO shows a reduction peak at about 509 °C. These peaks, however, could not be observed in the catalysts. In the case of catalysts made by excess-solution impregnation, all the catalysts show lower reduction temperature, which could be ascribed to the synergistic interaction between CuO and CeO_2. Further, it can be seen that the reduction property of copper-ceria catalysts is strongly affected by zeolite supports. Four primary peaks can be seen in these catalysts. As reported elsewhere [32,33], α peak at 196 °C is attributed to the reduction of highly dispersed CuO on CeO_2, which is more active for CO oxidation; β peaks at 220 and 242 °C represent the reduction of nanometer CuO dispersed on CeO_2. Besides, γ peaks at 275 and 281 °C can be ascribed to the reduction of Cu(I) species, whereas the presence of δ peak at 436 °C is a result of reduction of bulk CuO particles. From the results above, it can be concluded that the dispersed CuO on CeO_2 of NaX-ES contributed to the excellent catalytic performance in CO oxidation. In addition, the catalysts with β peaks, namely 4A-ES and NaY-ES, had worse catalytic activity. 5A-ES, which did not have either α or β peaks, exhibited the worst catalytic activity. It is interesting that for 4A-ES and NaX-ES, the loading of Cu and Ce was quite different, but the catalytic activity was similar, though the catalytic activity of NaX-ES was a little better. This could be explained by the fact that the Cu/Ce ratio in 4A-ES was similar to the catalysts with the best catalytic activity [34-36]. It may lead to the relatively good catalytic performance of 4A-ES. As for NaX-ES, it had larger BET surface area and pore volume, which facilitates the catalytic process. Besides, the α peak, which stood for the most active copper species dispersed on ceria, was examined in NaX-ES by H_2-TPR. Thereby, the large surface area and the active copper species contributed to the high catalytic activity of NaX-ES.

As for catalysts made by incipient wetness impregnation, two extra peaks—ε peak at 354 °C and ζ peak at 560 °C—were presented. According to the literature [14,33], the ε peak is due to a

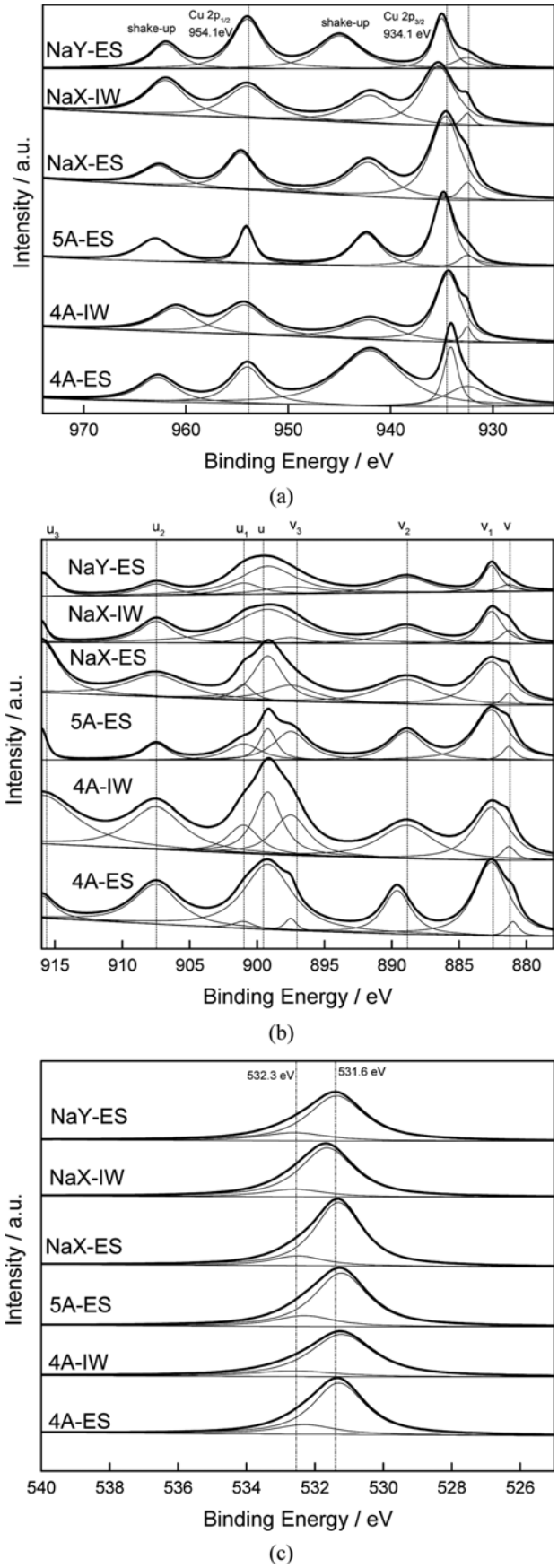

Fig. 7. XPS spectra of (a) Cu 2p, (b) Ce 3d and (c) O 1s in catalysts.

synergy between CeO_2 and Cu species; the ζ peak is attributed to reduction of surface CeO_2 species. ζ appeared at both 4A-IW and NaX-IW, which illustrated the generation of bulk CeO_2 caused by the incipient wetness impregnation. Furthermore, α peak in 4A-IW could be observed, indicating finely dispersed amorphous and crystalline CuO species strongly interacting with partial CeO_2 reduction at Cu-Ce interface, which contributed to the catalytic activity. corresponded Meanwhile, α peak, presented in NaX-ES, could not be seen in NaX-IW, suggesting the CuO species were more unevenly distributed on CeO_2 than those of NaX-ES. It can be proposed that zeolite supports have dramatic effects on the reducibility of catalysts. Also, the catalysts with α peak could exhibit better catalytic activity, as was shown in Fig. 1.

6. X-ray Photoelectron Spectroscopy (XPS)

XPS spectra of Cu 2p, Ce 3d and O1s binding energy of catalysts are shown in Fig. 7. For bulk copper oxides, the peak at 954.1 eV is ascribed to Cu 2p1/2. Besides, the binding energy of Cu 2p3/2 is centered at 932.5 eV for Cu^+ of Cu_2O, in contrast to 934.1 eV for Cu^{2+} of CuO with broad shake-up peaks around 940-945 eV as indicated in Fig. 7(a). As for the copper-ceria system, the reduced copper species assigned to Cu^+ at lower binding energy was identified as the well-dispersed copper oxide cluster, which strongly interacts with ceria and therefore was the main active site for CO oxidation [37]. The Ce 3d XPS spectra of samples are displayed in Fig. 7(b). These peaks stand for Ce 3d3/2 and Ce 3d5/2, which are labeled as u and v, respectively. The four intense peaks—v (882.5 eV), u (901.1 eV), v_3 (898.3 eV), u_3 (916.4 eV) as well as two weaker components v_2 (889.5 eV) and u_2 (908 eV)—could be ascribed to different Ce 4f electron configurations in the final state of Ce^{4+} species. In contrast, v_1 (885.7 eV) and u_1 (902.9 eV) could as attributed to one of the two possible electron configurations of the final state of Ce^{3+} species [38,39]. The O 1s spectra of catalysts are presented in Fig. 7(c), where peaks at 531.6 and 532.3 eV are observed. The peak at around 531.6 eV is characterized as the lattice oxygen of CeO_2 and CuO species, while the one at 532.3 eV might be assigned to the defect oxide or absorbed oxygen with low coordination situation [32]. All samples present the primary peaks of Cu 2p, Ce 3d and O 1s, which is in coordination with EDX, XRD and H_2-TPR results, suggesting the co-existence of different Cu, Ce species. Note that all catalysts exhibit similar XPS spectra, from which the difference between the catalysts can hardly be distinguished.

7. Catalytic Activity

The catalytic performance of 4A-ES, 4A-IW, NaX-ES and NaX-IW is shown in Fig. 8. The catalytic activity is quite different among samples. The catalytic performance of 4A-ES is slightly better than 4A-IW. The 50% CO conversion for 4A-ES and 4A-IW is almost the same, 127 °C and 129 °C, respectively. The 90% CO conversion for both 4A-ES and 4A-IW is almost 190 °C, though their XPS, XRD, N_2 adsorption-desorption and TPR profiles are quite different. The XPS profiles of 4A-ES and 4A-IW indicate that the same copper, ceria and oxygen species appear in all samples though the relative contents vary. The H_2-TPR results suggest the α peak in 4A-IW is much more observable than the one in 4A-ES. The similar catalytic activity of 4A-ES and 4A-IW could be due to the fact that 4A-ES has larger BET surface area and pore volume, which plays an important role in distributing the active species and pro-

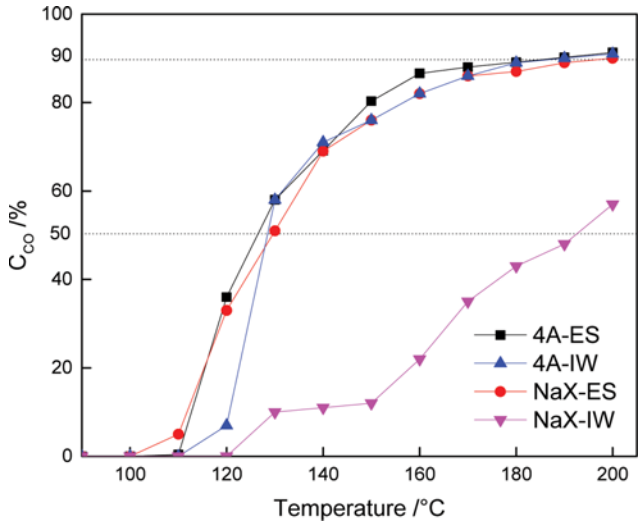

Fig. 8. Catalytic activity of catalysts.

moting the catalytic performance. For 4A-IW, although it had less surface area, the active copper species dispersed on ceria, examined by H_2-TPR results, compensated for the lessened surface area and randomly distributed metal species. In contrast, the catalytic performance of NaX-IW was much worse than that of NaX-ES. The 50% CO conversion for NaX-IW was 192 °C, while that for NaX-ES was 130 °C. The high catalytic activity of NaX-ES could be explained by the fact that the relatively large BET surface area and highly dispersed CuO on CeO_2 facilitated the reaction. As for NaX-IW, the drastic decrease in BET surface area and pore volume was responsible for the decrease in active sites, leading to low catalytic activity. Also, the disappearance of α peak, determined by H_2-TPR, also explained the poor catalytic activity of NaX-IW. It could be concluded that the catalytic activity of catalysts made by excess-solution impregnation was generally better than that of catalysts made by incipient wetness impregnation.

CONCLUSIONS

The effects of zeolite support and impregnation method on the catalytic activity of copper-ceria catalysts for CO oxidation have been studied in this work. The catalytic activity of catalysts made by excess-solution increases in the order of 5A-ES<NaY-ES<NaX-ES≈4A-ES. The catalytic activity of catalysts made by incipient wetness impregnation was generally worse than that of catalysts made by excess-solution impregnation, examined by the T_{50} of 4A-IW and NaX-IW at 128 and 192 °C, in comparison with that of 4A-ES and NaX-ES at 127 and 129 °C, respectively. The high catalytic activity of NaX-ES could be ascribed to the large surface area of 365 m^2 g^{-1} and the highly dispersed copper species on ceria, as indicated by α peak at 196 °C in TPR results.

ACKNOWLEDGEMENTS

We gratefully acknowledge the financial support of the National Natural Science Foundation of China (Grant No. 21176086 and 21376101), Science and Technology Planning Project of Guangdong Province, China (No. 2013B010403002) and Fundamental Research Funds for the Central University (No. 2015Z2116).

REFERENCES

1. K. An, S. Alayoglu, N. Musselwhite, S. Plamthottam, G. Melaet, A. E. Lindeman and G. A. Somorjai, *J. Am. Chem. Soc.*, **135**, 16689 (2013).
2. J.-N. Lin and B.-Z. Wan, *Appl. Catal. B: Environ.*, **41**, 83 (2003).
3. M. S. Chen, Y. Cai, Z. Yan, K. K. Gath, S. Axnanda and D. W. Goodman, *Surface Sci.*, **601**, 5326 (2007).
4. K. Qian, Z. Qian, Q. Hua, Z. Jiang and W. Huang, *Appl. Surface Sci.*, **273**, 357 (2013).
5. X. Liu, J. Lu, K. Qian, W. Huang and M. Luo, *Journal of Rare Earths.*, **27**, 418 (2009).
6. Y. Liu, Q. Fu and M. F. Stephanopoulos, *Catal. Today*, **93-95**, 241 (2004).
7. N. C. Pérez, E. E. Miró and J. M. Zamaro, *Catal. Today*, **213**, 183 (2013).
8. A. Gurbani, J. L. Ayastuy, M. P. González-Marcos, J. E. Herrero, J. M. Guil and M. A. Gutiérrez-Ortiz, *Int. J. Hydrogen Energy*, **34**, 547 (2009).
9. X. Zheng, S. Wang, S. Wang, S. Zhang, W. Huang and S. Wu, *Catal. Commun.*, **5**, 729 (2004).
10. A. Manasilp and E. Gulari, *Appl. Catal. B: Environ.*, **37**, 17 (2002).
11. H. Zhu, C. Liang, W. Yan, S. H. Overbury and S. Dai, *J. Phys. Chem. B.*, **110**, 10842 (2006).
12. L. Kiwi-Minsker, I. Yuranov, B. Siebenhaar and A. Renken, *Catal. Today*, **54**, 39 (1999).
13. W. Han, P. Zhang, Z. Tang and G. Lu, *Process Safety and Environmental Protection.*, **92**, 822 (2014).
14. N. C. Pérez, E. E. Miró and J. M. Zamaro, *Appl. Catal. B: Environ.*, **129**, 416 (2013).
15. H. Igarashi, H. Uchida, M. Suzuki, Y. Sasaki and M. Watanabe, *Appl. Catal. A: Gen.*, **159**, 159 (1997).
16. E. Kolobova, A. Pestryakov, A. Shemeryankina, Y. Kotolevich, O. Martynyuk, H. J. Tiznado Vazquez and N. Bogdanchikova, *Fuel*, **138**, 65 (2014).
17. D. Verboekend, T. C. Keller, S. Mitchell and J. Pérez-Ramírez, *Adv. Funct. Mater.*, **23**, 1923 (2013).
18. H. L. Tidahy, S. Siffert, J. F. Lamonier, R. Cousin, E. A. Zhilinskaya, A. Aboukaïs, B. L. Su, X. Canet, G. De Weireld, M. Frère, J. M. Giraudon and G. Leclercq, *Appl. Catal. B: Environ.*, **70**, 377 (2007).
19. B.-H. Jeong, K.-I. Sotowa and K. Kusakabe, *J. Membr. Sci.*, **224**, 151 (2003).
20. I. Rosso, C. Galletti, G. Saracco, E. Garrone and V. Specchia, *Appl. Catal. B: Environ.*, **48**, 195 (2004).
21. M. Bowker, A. Nuhu and J. Soares, *Catal. Today*, **122**, 245 (2007).
22. U. Junges, W. Jacobs, I. Voigt-Martin, B. Krutzsch and F. Schuth, *J. Chem. Soc., Chem. Commun.*, 2283 (1995).
23. J. M. C. Soares, P. Morrall, A. Crossley, P. Harris and M. Bowker, *J. Catal.*, **219**, 17 (2003).
24. W.-w. Bao, H.-f. Zou, S.-c. Gan, X.-c. Xu, G.-j. Ji and K.-y. Zheng, *Chemical Research in Chinese Universities*, **29**, 126 (2013).
25. E. Erdem, N. Karapinar and R. Donat, *J. Colloid Interface Sci.*, **280**, 309 (2004).

26. E. Z. Hegazy, I. H. Abdelmaksod and S. A. Kosa, *CLEAN – Soil, Air, Water.*, **42**, 775 (2014).
27. D. Gamarra, A. L. Cámara, M. Monte, S. B. Rasmussen, L. E. Chinchilla, A. B. Hungría, G. Munuera, N. Gyorffy, Z. Schay, V. C. Corberán, J. C. Conesa and A. Martínez-Arias, *Appl. Catal. B: Environ.*, **130-131**, 224 (2013).
28. V. P. Valtchev, L. Tosheva and K. N. Bozhilov, *Langmuir*, **21**, 10724 (2005).
29. S. N. Azizi, A. R. Dehnavi and A. Joorabdoozha, *Mater. Res. Bulletin.*, **48**, 1753 (2013).
30. P. Serp and E. Castillejos, *ChemCatChem.*, **2**, 41 (2010).
31. F. Pinna, *Catal. Today*, **41**, 129 (1998).
32. P. Zhu, M. Liu and R. Zhou, *Indian Journal of Chemistry-Part A Inorganic Physical Theoretical and Analytical*, **51**, 1529 (2012).
33. C. Gu, S. Lu, J. Miao, Y. Liu and Y. Wang, *Int. J. Hydrogen Energy*, **35**, 6113 (2010).
34. D. Kim and J. Cha, *Catal. Lett.*, **86**, 107 (2003).
35. S. Zeng, W. Zhang, M. Śliwa and H. Su, *Int. J. Hydrogen Energy*, **38**, 3597 (2013).
36. M.-F. Luo, J.-M. Ma, J.-Q. Lu, Y.-P. Song and Y.-J. Wang, *J. Catal.*, **246**, 52 (2007).
37. Y. Gao, K. Xie, W. Wang, S. Mi, N. Liu, G. Pan and W. Huang, *Catal. Sci. Technol.*, **5**, 1568 (2015).
38. F. Bin, X. Wei, B. Li and K. S. Hui, *Appl. Catal. B: Environ.*, **162**, 282 (2015).
39. L. Katta, P. Sudarsanam, G. Thrimurthulu and B. M. Reddy, *Appl. Catal. B: Environ.*, **101**, 101 (2010).